Research Article Vol. 24, No. 19 | 19 Sep 2016 | OPTICS EXPRESS 22177

Optics EXPRESS

Liquid microlenses and waveguides from bulk nematic birefringent profiles

MIHA ČANČULA,[1,*] MIHA RAVNIK,[1,2] IGOR MUŠEVIČ,[1,2] AND SLOBODAN ŽUMER[1,2]

[1] *Faculty of Mathematics and Physics, University of Ljubljana, Jadranska 19, 1000 Ljubljana, Slovenia*
[2] *Jožef Stefan Institute, Jamova cesta 39, 1000 Ljubljana, Slovenia*
[*] *miha.cancula@fmf.uni-lj.si*
http://softmatter.fmf.uni-lj.si/

Abstract: We demonstrate polarization-selective microlensing and waveguiding of laser beams by birefringent profiles in bulk nematic fluids using numerical modelling. Specifically, we show that radial escaped nematic director profiles with negative birefringence focus and guide light with radial polarization, whereas the opposite – azimuthal – polarization passes through unaffected. A converging lens is realized in a nematic with negative birefringence, and a diverging lens in a positive birefringence material. Tuning of such single-liquid lenses by an external low-frequency electric field and by adjusting the profile and intensity of the beam itself is demonstrated, combining external control with intrinsic self-adaptive focusing. Escaped radial profiles of birefringence are shown to act as single-liquid waveguides with a single distinct eigenmode and low attenuation. Finally, this work is an approach towards creating liquid photonic elements for all-soft matter photonics.

OCIS codes: (160.3710) Liquid crystals; (160.1190) Anisotropic optical materials; (260.1440) Birefringence; (260.5430) Polarization; (260.5950) Self-focusing.

References and links

1. D. R. Smith, W. J. Padilla, D. C. Vier, S. C. Nemat-Nasser, and S. Schultz, "Composite medium with simultaneously negative permeability and permittivity," Phys. Rev. Lett. **84**, 4184–4187 (2000).
2. R. A. Shelby, D. R. Smith, and S. Schultz, "Experimental verification of a negative index of refraction," Science **292**, 77–79 (2001).
3. J. B. Pendry, D. Schurig, and D. R. Smith, "Controlling electromagnetic fields," Science **312**, 1780–1782 (2006).
4. J. B. Pendry, "Negative refraction makes a perfect lens," Phys. Rev. Lett. **85**, 3966–3969 (2000).
5. S. J. Woltman, G. D. Jay, and G. P. Crawford, "Liquid-crystal materials find a new order in biomedical applications," Nat. Mater. **6**, 929 (2007).
6. B. F. Grewe, F. F. Voigt, M. van 't Hoff, and F. Helmchen, "Fast two-layer two-photon imaging of neuronal cell populations using an electrically tunable lens," Biomed. Opt. Express **2**, 2035 (2011).
7. H.-S. Chen and Y.-H. Lin, "An endoscopic system adopting a liquid crystal lens with an electrically tunable depth-of-field," Opt. Express **21**, 18079–18088 (2013).
8. H.-C. Lin, M.-S. Chen, and Y.-H. Lin, "A review of electrically tunable focusing liquid crystal lenses," Trans. Electr. Electron. Mater. **12**, 234 (2011).
9. O. Pishnyak, S. Sato, and O. D. Lavrentovich, "Electrically tunable lens based on a dual-frequency nematic liquid crystal," Appl. Opt. **45**, 4576 (2006).
10. M. Kasano, M. Ozaki, K. Yoshino, D. Ganzke, and W. Haase, "Electrically tunable waveguide laser based on ferroelectric liquid crystal," Appl. Phys. Lett. **82**, 4026 (2003).
11. N. Glazar, C. Culbreath, Y. Li, and H. Yokoyama, "Switchable liquid-crystal phase-shift mask for super-resolution photolithography based on Pancharatnam–Berry phase," Appl. Phys. Express **8**, 116501 (2015).
12. F. Serra, M. A. Gharbi, Y. Luo, I. B. Liu, N. D. Bade, R. D. Kamien, S. Yang, and K. J. Stebe, "Curvature-driven, one-step assembly of reconfigurable smectic liquid crystal "compound eye" lenses," Adv. Opt. Mater. **3**, 1287 (2015).
13. T. Krupenkin, S. Yang, and P. Mach, "Tunable liquid microlens," Appl. Phys. Lett. **82**, 316–318 (2003).
14. N. Chronis, G. Liu, K.-H. Jeong, and L. Lee, "Tunable liquid-filled microlens array integrated with microfluidic network," Opt. Express **11**, 2370 (2003).
15. H. Ren and S.-T. Wu, *Introduction to Adaptive Lenses* (Wiley, 2012).
16. P. G. de Gennes and J. Prost, *The Physics of Liquid Crystals, Second Edition* (Oxford University Press, 1995).
17. I. Muševič, "Liquid-crystal micro-photonics," Liq. Cryst. Rev. **4**, 1 (2016).
18. I. C. Khoo, "Nonlinear optics, active plasmonics and metamaterials with liquid crystals," Prog. Quant. Electron. **38**, 77 (2014).

#270613 http://dx.doi.org/10.1364/OE.24.022177
Journal © 2016 Received 19 Jul 2016; revised 8 Sep 2016; accepted 8 Sep 2016; published 15 Sep 2016

Optics EXPRESS

19. I. Muševič, "Forces in nematic liquid crystals: from nanoscale interfacial forces to long-range forces in nematic colloids," Liq. Crys. **36**, 639–647 (2009).
20. H. J. Eichler and R. Macdonald, "Flow-alignment and inertial effects in picosecond laser-induced reorientation phenomena of nematic liquid crystals," Phys. Rev. Lett. **67**, 2666–2669 (1991).
21. N. Kamanina, S. Putilin, and D. Stasel'ko, "Nano-, pico- and femtosecond study of fullerene-doped polymer-dispersed liquid crystals: holographic recording and optical limiting effect," Synthetic Met. **127**, 129 – 133 (2002).
22. L. Cattaneo, M. Savoini, I. Muševič, A. Kimel, and T. Rasing, "Ultrafast all-optical response of a nematic liquid crystal," Opt. Express **23**, 14010 (2015).
23. M. Humar, M. Ravnik, S. Pajk, and I. Muševič, "Electrically tunable LC optical microresonators," Nat. Photonics **3**, 595–600 (2009).
24. M. Humar and I. Muševič, "3D microlasers from self-assembled cholesteric LC microdroplets," Opt. Express **18**, 26995–27003 (2010).
25. K. Peddireddy, V. S. R. Jampani, S. Thutupalli, S. Herminghaus, C. Bahr, and I. Muševič, "Lasing and waveguiding in smectic A liquid crystal optical fibers," Opt. Express **21**, 30233–30242 (2013).
26. L. Marrucci, C. Manzo, and D. Paparo, "Optical spin-to-orbital angular momentum conversion in inhomogeneous anisotropic media," Phys. Rev. Lett. **96**, 163905 (2006).
27. H. Coles and S. Morris, "Liquid-crystal lasers," Nat. Photonics **4**, 676–685 (2010).
28. P. J. W. Hands, S. M. Morris, T. D. Wilkinson, and H. J. Coles, "Two-dimensional liquid crystal laser array," Opt. Lett. **33**, 515–517 (2008).
29. C. Loussert, U. Delabre, and E. Brasselet, "Manipulating the orbital angular momentum of light at the micron scale with nematic disclinations in a liquid crystal film," Phys. Rev. Lett. **111**, 037802 (2013).
30. M. Wahle and H.-S. Kitzerow, "Liquid crystal assisted optical fibres," Opt. Express **22**, 262 (2014).
31. K. A. Rutkowska, K. Milenko, O. Chojnowska, R. Dabrowski, and T. R. Woli´nski, "Light propagation mechanism switching in a liquid crystal infiltrated microstructured polymer optical fibre," Opto-Electron. Rev. **23**, 34 (2015).
32. D. C. Zografopoulos, R. Asquini, E. E. Kriezis, A. d'Alessandro, and R. Beccherelli, "Guided-wave liquid-crystal photonics," Lab. Chip. **12**, 3598 (2012).
33. D. Kleman and O. D. Lavrentovich, *Soft Matter Physics: An Introduction* (Springer, 2003).
34. G. Assanto, *Nematicons: Spatial Optical Solitons in Nematic Liquid Crystals*, Wiley Series in Pure and Applied Optics (Wiley, 2012).
35. A. Piccardi, A. Alberucci, N. Kravets, O. Buchnev, and G. Assanto, "Power-controlled transition from standard to negative refraction in reorientational soft matter," Nat. Commun. **5**, 5533 (2014).
36. R. Barboza, U. Bortolozzo, G. Assanto, E. Vidal-Henriquez, M. G. Clerc, and S. Residori, "Harnessing optical vortex lattices in nematic liquid crystals," Phys. Rev. Lett. **111**, 093902 (2013).
37. A. Martinez and I. I. Smalyukh, "Light-driven dynamic Archimedes spirals and periodic oscillatory patterns of topological solitons in anisotropic soft matter," Opt. Express **23**, 4591 (2015).
38. E. Brasselet, N. Murazawa, H. Misawa, and S. Juodkazis, "Optical vortices from liquid crystal droplets," Phys. Rev. Lett. **103**, 103903 (2009).
39. M. Čančula, M. Ravnik, and S. Žumer, "Generation of vector beams with liquid crystal disclination lines," Phys. Rev. E **90**, 022503 (2014).
40. E. Brasselet, "Singular optical reordering of liquid crystals using Gaussian beams," J. Opt. **12**, 124005 (2010).
41. T. Porenta, M. Ravnik, and S. Žumer, "Complex field-stabilized nematic defect structures in Laguerre-Gaussian optical tweezers," Soft Matter **8**, 1865–1870 (2012).
42. U. Tkalec, M. Ravnik, S. Žumer, and I. Muševič, "Vortexlike topological defects in nematic colloids: Chiral colloidal dimers and 2D crystals," Phys. Rev. Lett. **103**, 127801 (2009).
43. M. Nikkhou, M. Škarabot, S. Čopar, M. Ravnik, S. Žumer, and I. Muševič, "Light-controlled topological charge in a nematic liquid crystal," Nat. Phys. **11**, 183 (2015).
44. Q. Zhan, "Cylindrical vector beams: from mathematical concepts to applications," Adv. Opt. Photon. **1**, 1–57 (2009).
45. Y. Kozawa and S. Sato, "Generation of a radially polarized laser beam by use of a conical Brewster prism," Opt. Lett. **30**, 3063–3065 (2005).
46. S.-W. Shih-Wei Ko, C.-L. Ting, A. Y.-G. Fuh, and T.-H. Lin, "Polarization converters based on axially symmetric twisted nematic liquid crystal," Opt. Express **18**, 3601–3607 (2010).
47. M. Ravnik and S. Žumer, "Landau-de Gennes modelling of nematic liquid crystal colloids," Liq. Cryst. **36**, 1201–1214 (2009).
48. A. Taflove and S. C. Hagness, *Computational Electrodynamics: The Finite-Difference Time-Domain Method*, Artech House Antennas and Propagation Library (Artech House, 2005).
49. E. Hecht, *Optics* (Addison-Wesley Longman, 2002).
50. ISO 11146-1:2005, *Test methods for laser beam widths, divergence angles and beam propagation ratios* (International Organization for Standardization, 2005).
51. R. Dorn, S. Quabis, and G. Leuchs, "Sharper focus for a radially polarized light beam," Phys. Rev. Lett. **91**, 233901 (2003).

1. Introduction

Micro-manipulation of the flow-of-light is today a major fundamental and technological challenge, with implications including fundamental technological challenges in metamaterials design [1, 2], transformation optics [3], and sub-wavelength microscopy [4]. Lenses are among the core elements needed for light manipulation, and one of the major challenges is to achieve tunability on a microscopic scale. Tunable lenses are used in multi-photon microscopy, providing fast focus shifting of the scanning beam [5, 6], as well as in endoscopy where tunability and small size are important [7]. Such lenses can be based on liquid crystals [8–12], electrowetting [13], or elastomer membranes [14], while the tuning is typically achieved by applying an external electric field [15].

Nematic liquid crystals (NLCs) are known photonic materials, with their key differentiator being the easily tunable optical birefringence [16–18], which can be designed and manipulated over multiple orders of magnitude in length scales, from 10 nm to 100 µm [19], and on time scales ranging from milliseconds down to picoseconds [20–22]. This broad variability allows for design of various photonic elements, including microresonators [23, 24], waveguides [25], polarization converters [26], and micro-lasers [10, 27]. Photonic elements are typically realized in layered geometries [28, 29], or in double emulsions [24, 25]. Liquid crystals are often used as a component in fibers and other waveguides, where they enable external control and tuning of the optical parameters [30–32].

Light and liquid crystals birefringence are inherently mutually coupled. On one hand, the birefringence affects the flow-of-light while on the other hand, the dielectric coupling between the light field and the induced dipoles of the nematic molecules change the birefringence profile of the nematic [16, 33]. Particularly, this coupling can become very relevant at strongly varying nematic profiles or at higher light intensities. The coupling between these two effects give rise to interesting phenomena such as nematicons [34], tunable negative refraction [35] and self-induced optical vortices [29, 36, 37]. However, today most LC photonic works are performed in the regimes where this coupling is rather weak, therefore ignoring either reorientation due to light field [26, 38, 39] or the effect of the liquid crystal profile on incident beams [40, 41].

Structurally, nematic liquid crystals are soft materials where molecules have a long-range orientational order, but no long-range positional order. This ordering is characterized by their average orientation, called the director **n**, and the nematic degree of order S. The optical axis in nematics is parallel to the director and can vary in space and time. In the equilibrium state, the nematic director is uniform, and any deformations of the director reduce the freedom of molecules and thus increase the free energy of the system. However, external fields or surfaces can impose a different profile. Placing the NLC into a capillary with suitably-treated walls produces the so-called "escaped" profile, where molecules are perpendicular to the walls, but parallel to the capillary axis at the center. Such a profile is shown in Fig. 1.

Radial escaped nematic profiles are commonly observed as the line structure in nematic capillaries [33], in the form of escaped loops in colloidal systems [42] or as solitons in various confined systems [43]. In such a line structure, the nematic director continuously changes from being aligned along the line in the centre of the profile and perpendicular in the radial direction at the outside of the profile, as shown in Fig. 1. This profile is nonsingular, as the nematic director is well-defined and continuous everywhere. Optically, the ordinary and extraordinary refractive indices are uniform, but the principal axis varies in the direction perpendicular to the escaped radial line. The radial symmetry of an escaped profile can be matched by a radially polarized light beam [44]. Such beams can be generated using liquid crystal defect structures [26, 39], conical Brewster prisms [45], or phase modulators [46]. In such a setup, the incident polarization is always extraordinary, and the corresponding refractive index varies with the distance from the axis. The light observed the ordinary index at the axis, and the extraordinary index near the edge of the escaped profile. The refractive index contrast, and with it the lensing effect, comes from the liquid crystal ordering itself, meaning that it can be realized in single-component bulk liquid crystals. To achieve converging lenses, the index of refraction needs to be greater at the center than near the capillary wall, which requires a material with negative birefringence, whereas for diverging lens more common positive birefringence nematic materials need to be used. The azimuthal polarization, which is orthogonal to the radial one, observes a uniform refractive index and is unaffected by the director profile. The focusing effects demonstrated in the paper are thus highly polarization dependent.

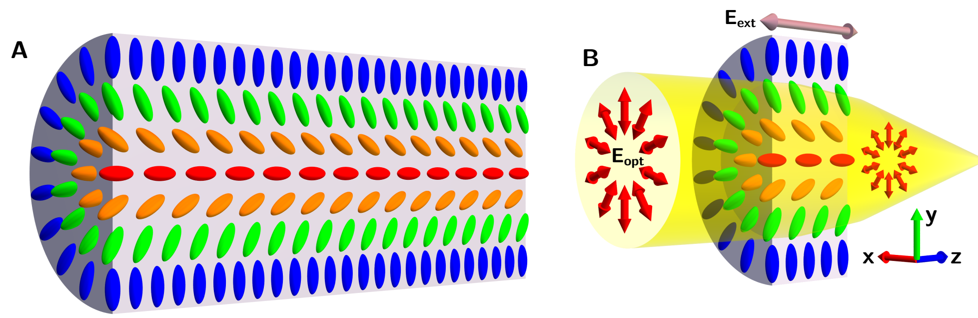

Fig. 1. Radial escaped nematic line as a photonic element. (A) An escaped profile of the nematic liquid crystal. Away from the axis, molecules are perpendicular to the escaped line, and continuously transition to a parallel orientation at the axis. (B) Radially polarized light (polarization illustrated by red arrows) propagating through a short segment of an escaped director profile observed a radially-dependent refractive index, resulting in focusing and lensing, while the polarization profile is preserved. The optical electric field E_{opt}, external electric field E_{ext}, and the chosen coordinate system are shown with arrows.

In this paper, we show that birefringent escaped director profiles in nematics can be used as tunable self-adaptive photonic elements, specifically as single-component liquid microlenses and waveguides for Laguerre-Gaussian light beams. The variable angle of the director with respect to the incident polarization causes the light to observe a spatially-dependent index of refraction, resulting in beam focusing and beam guiding. The light retardation imposed by such fluid photonic elements is shown to be dependent on the material birefringence and its spatial profile, making such elements polarization dependent. Focusing in microlenses is shown to be tunable with the beam intensity, demonstrating an interesting self-adaptive lensing dependence. We combine the self-adapting behavior with an external electric field, further tuning the symmetry and profile of the lens to achieve designable focusing properties. Finally, we show that the focusing effect can be also used for waveguiding, transporting the light along a single-fluid birefringence profile. Such waveguides have a distinct propagation eigenmode with a fixed polarization, indicating the possibility of using escaped profiles as polarization-dependent beam splitters.

2. Theory and numerical modelling

Light field and the material birefringence field are inherently coupled in nematic fluids via the material dielectric permittivity, with the change in the either of two fields affecting the other. Methodologically, this mutual coupling requires rather challenging (and often ignored) coupled input on light propagation and the nematic orientational ordering. We propose here an approach where we combine the established mesoscopic free-energy based modelling of liquid crystal and solving Maxwell's equations for of the light field, where importantly the nematic and the light field mutually adapt to one another. Specifically, we describe the nematic orientation by using phenomenological Landau-de Gennes (LdG) free energy relaxation [47], and combine it

Optics EXPRESS

with the custom-developed finite-difference time-domain (FDTD) method [39, 48] for modelling the propagation of light in an arbitrary spatially varying optically anisotropic material. This combined approach gives a strong theoretical predictive and modelling methodological tool capable of describing in full the mutual coupling effects between light and birefringence in arbitrary nematic fluid-based photonic geometry.

The time-evolution of **E** and **H** is computed directly using the Maxwell's equations

$$\varepsilon \frac{\partial \mathbf{E}}{\partial t} = \nabla \times \mathbf{H}\,, \qquad \mu \frac{\partial \mathbf{H}}{\partial t} = -\nabla \times \mathbf{E}\,.$$

In order to support arbitrary anisotropic media, we use the full 3D FDTD method, where all six components of **E** and **H** are considered. The electric and magnetic fields are updated alternatively, so that the magnetic field is computed with a half-step delay with respect to the electric field. This alternation, together with computing the electric and magnetic field at different positions, improves accuracy with no loss of performance. Our FDTD software uses a nonstandard lattice, sacrificing some of the performance in favor of stability and compatibility with the liquid crystal relaxation method [39].

Equilibrium ordering of the liquid crystal is obtained by minimization of the Landau-de Gennes free energy functional

$$F = \int_V \Big(\underbrace{\frac{1}{2} L \frac{\partial Q_{ij}}{\partial x_i}\frac{\partial Q_{ij}}{\partial x_i}}_{\text{elasticity}} - \underbrace{\frac{1}{3}\varepsilon_0 \varepsilon_{\mathrm{a}}^{\mathrm{mol,opt}} \langle E_i^{\mathrm{opt}} Q_{ij} E_j^{\mathrm{opt}}\rangle}_{\text{coupling with light}} - \underbrace{\frac{1}{3}\varepsilon_0 \varepsilon_{\mathrm{a}}^{\mathrm{mol,ext}} \langle E_i^{\mathrm{ext}} Q_{ij} E_j^{\mathrm{ext}}\rangle}_{\text{coupling with external field}} \Big) \mathrm{d}V +$$
$$+ \int_V \Big(\underbrace{\frac{1}{2} A(T)\,\mathrm{Tr}\,Q^2 + \frac{1}{3} B\,\mathrm{Tr}\,Q^3 + \frac{1}{4} C (\mathrm{Tr}\,Q^2)^2}_{\text{nematic-isotropic transition}} \Big) \mathrm{d}V + \int_{\partial V} \Big(\underbrace{\frac{1}{2} W (Q - Q_0)^2}_{\text{surface anchoring}} \Big) \mathrm{d}S$$

where the first term describes the elastic free energy due to spatial variations of the director, the second and third term describe the coupling between the liquid crystal and an electric or optical field, the fourth term is the Landau expansion describing the temperature-driven phase transition between nematic and isotropic state, and the fifth term the surface anchoring on confining surfaces. The dielectric coupling constant $\varepsilon_{\mathrm{a}}^{\mathrm{mol}} = \varepsilon_{\mathrm{A}}/S = (\varepsilon_{\parallel} - \varepsilon_{\perp})/S$ is the frequency-dependent molecular dielectric anisotropy. We have explicitly separated the contributions from a low-frequency external electric field E_{ext} and from the optical electric field E_{opt} because $\varepsilon_{\mathrm{a}}^{\mathrm{mol}}$ differs by several orders of magnitude between the optical frequencies and the low frequency of the external electric field. Other possible contributions to the free energy, such as chirality, flexoelectricity and magnetic coupling could also be incorporate into the approach if needed.

We model the mutual interaction between light and liquid crystal by alternating between steps of liquid crystal relaxation (*LdG steps*) and steps of solving Maxwell's equations (*FDTD steps*), as illustrated by the flowchart in Fig. 2. The iterative approach effectively separates the time scales into an effective multiple timescale algorithm. Additional conversions are needed when switching from FDTD to LdG steps and vice versa. Maxwell's equations for birefringent materials contain the inverse dielectric permittivity tensor $(\varepsilon^{-1})_{ij}$, which is calculated from the liquid crystal order parameter tensor Q_{ij}. On the other hand, LdG relaxation is affected by the light *intensity tensor* $I_{ij} = \langle E_i E_j \rangle$ obtained by averaging the products of electric field components over one wave period at every point in space. Optimal numbers of repetitions for light and relaxation steps depend on the system size; notably, light should traverse the simulation cell in each iteration to reach the steady state, while there is no methodological restriction on the number of relaxation steps. The alternation is repeated until a steady-state solution is achieved. The numerical method is highly parallel and runs entirely on GPUs, which enables us to accurately model relatively large systems quickly. A typical run takes around a day on a machine with 4 Nvidia Titan GPUs.

Optics EXPRESS

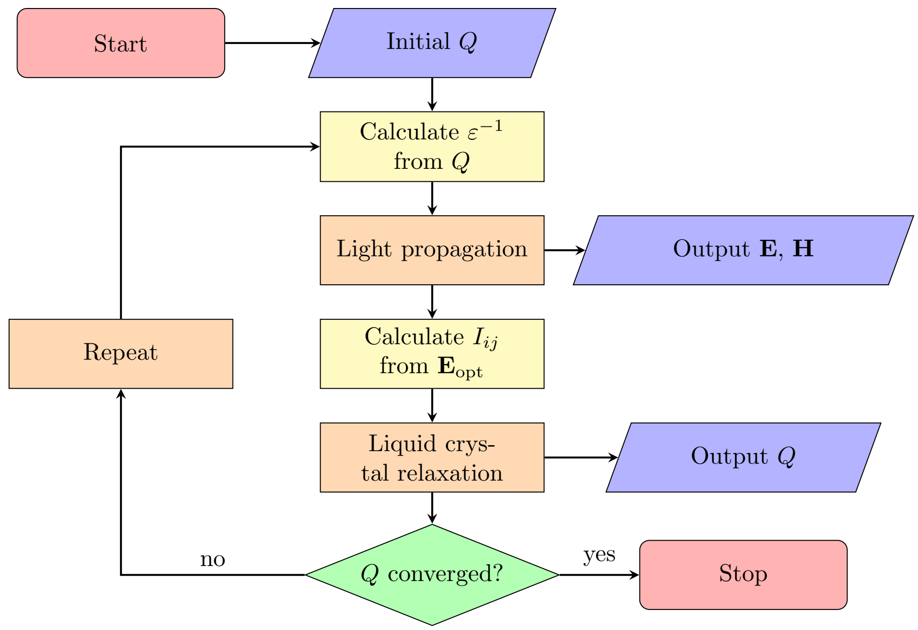

Fig. 2. Numerical algorithm flowchart.

The following numerical parameters are used in our modelling: wavelength $\lambda = 390\,\mathrm{nm}$, optical birefringence $\Delta n = -0.05$, lens thickness $5\,\mu\mathrm{m}$, escaped profile diameter $12\,\mu\mathrm{m}$ for lenses and $6\,\mu\mathrm{m}$ for waveguides, low-frequency dielectric anisotropy $\varepsilon_\mathrm{A} = -8.0$. The one-constant approximation is used, with the single elastic constant equal to $L = 40\,\mathrm{pN}$. The simulation box is three-dimensional, with size equal to $12\,\mathrm{nm} \times 12\,\mathrm{nm} \times 24\,\mathrm{nm}$, while the incident beam is propagating mainly in the z direction. We take the simulation box to impose distinct anchoring at the boundaries in order to stabilise the escaped radial profile, with the anchoring strength $W = 10^{-5}\,\mathrm{J/m^2}$ at the z boundary and $W = 10^{-3}\,\mathrm{J/m^2}$ at the x and y boundaries. Zero absorption of light in the material is assumed. For electric field tuning of the lenses, we use strenghts of up to $E_\mathrm{ext} = 1\,\mathrm{V}/\mu\mathrm{m}$, which is sufficient to overcome the nematic elasticity. In order to obtain a similar effect on the liquid crystal, the electric field in light is stronger, up to $10\,\mathrm{V}/\mu\mathrm{m}$, because the dielectric anisotropy is much smaller at optical frequencies. The desired electric field is achieved with a Laguerre-Gaussian beam with radius $3\,\mu\mathrm{m}$ and total power P of approximately $1\,\mathrm{W}$. Such laser power is at the high-end for typical lasers and optical tweezers used for liquid crystal research, but it is spread over a relatively large focus spot.

Sensible generic values are chosen for the light and material parameters, as their values have no qualitative impact on the results. The competition between nematic elasticity and light-imposed reorientation is the driving force behind the phenomena described here, and the exact value of light-field parameters need to be considered and used relative to the effective strength of the nematic elasticity, as well as relative to the optical anisotropy at low and high frequencies. The wavelength of light is chosen to provide a suitable amount of beam divergence inside the lenses and waveguides. The no-absorption regime, apart from being easier to implement numerically, is used in order to discern the distinct waveguide modes and study the waveguide performance without additional losses caused by absorption.

Optics EXPRESS

3. Results

3.1. Microlensing

A radially polarized light beam is sent along a segment of a nematic escaped profile and lensing is observed. In an ideal converging lens, the phase retardation varies with radial distance as $\Delta(r) = r^2/2\lambda f$, where f is the focal length of the lens [49]. In escaped profiles the profile is instead proportional to $(R^2 - r^2)/(R^2 + r^2)$ [33], which leads to a less clearly defined focal point and a spot size above the diffraction limit. It is thus desirable to reorder the liquid crystal to optimize the profile and obtain a radial profile of the refractive index closer to the radius-squared relation above. We employ the light beam itself as well as an external electric field for tuning the nematic profile. As the beam is travelling in the z direction, we define the *director angle* θ as the angle between the local nematic director and the z axis. In the escaped profile in the absence of electric fields, the director angle is 0° at the axis, and continuously changes to 90° at the boundary of the profile. Assuming a negative-birefringence nematic, a lower director angle corresponds to a higher index of refraction, and vice versa.

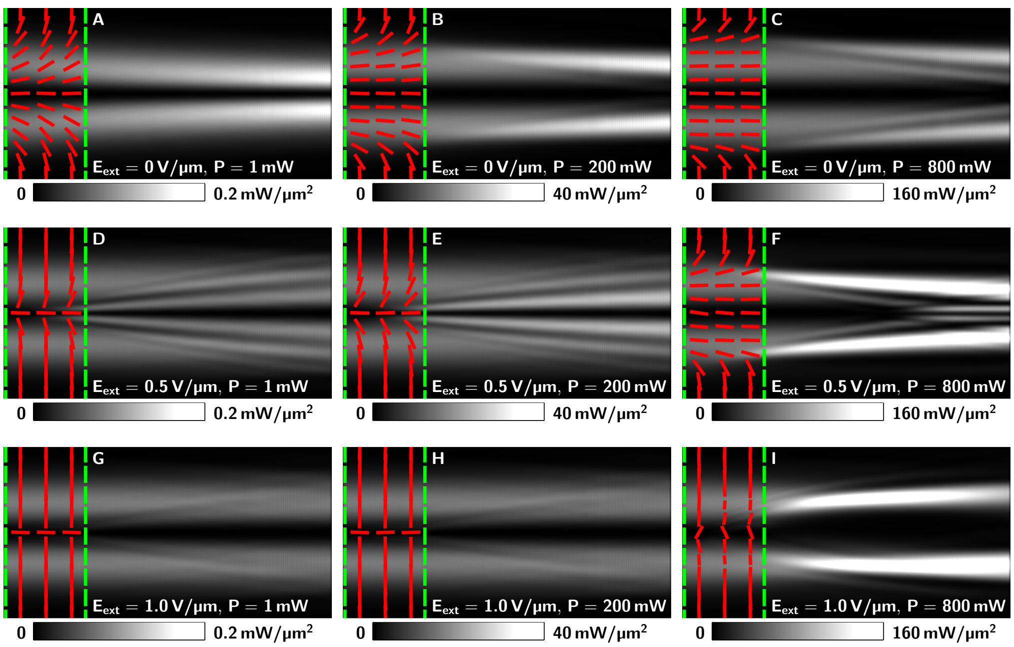

Fig. 3. Lensing of high-intensity beams on an escaped disclination line in the presence of an external electric field. Shades of gray show the local light intensity with the scale given by colorbar under each image, red lines show the local director profile inside the liquid crystal lens, while green dashed lines mark the lens boundary. (A-I) Competition between elastic forces, optical fields of the beam with power P and an external electric field E_{ext} produces a rich variety of lensing patterns. Interesting director structures form in medium-strength external fields ($E_{\text{ext}} \sim 0.5$ V/µm), where beam power P has a strong effect on the director profile and lensing. As the external field strength is increased, the structure transforms into a completely radial profile with a defect line at the axis. In all cases, light intensity is almost completely axially symmetric, as is the director angle of escape and with it the observed index of refraction.

Both the light beams themselves and external fields affect the ordering of the liquid crystal, resulting in different focusing properties, as shown in Fig. 3. Since the polarization of light is perpendicular to the external electric field, they have opposite effects on the local liquid

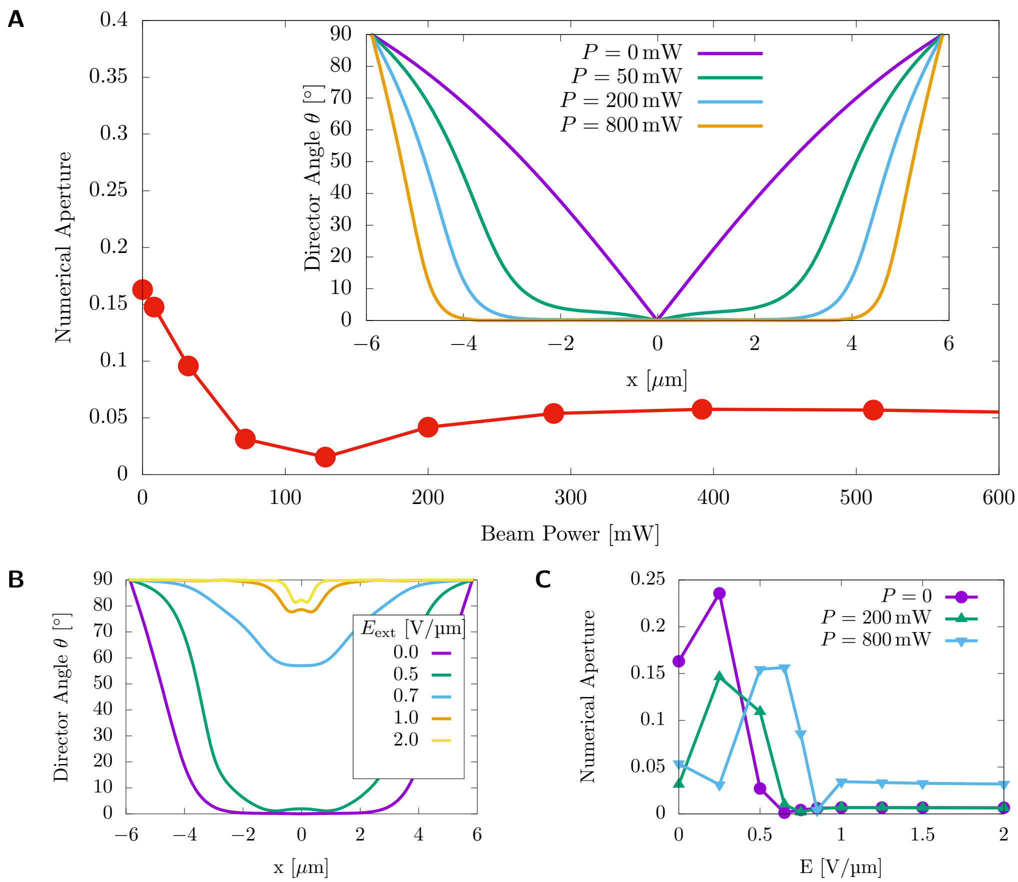

Fig. 4. (A) Numerical aperture of the lens as a function of beam power in the absence of an external electric field. We see that the numerical aperture is highest for weak beams, then quickly drops as power is increased, and finally stabilizes at a lower value for high beam powers. The inset shows the director angle profiles at different beam powers. Strong beams reduce the director angle, resulting in a wide area where the director is parallel to the escaped line axis. (B) Director angle of escape at different external field strengths and a strong (P = 800 mW) light beam. When the external field is weak, below 0.5 V/μm, the director is mostly in the z direction. As the external field is increased, it gradually changes and the director becomes aligned in the xy plane. (C) The numerical aperture of the lens at different external field strengths and beam powers. The numerical aperture is highest at a distinct external field strength E_{ext}, which depends on the beam power. Notably, changing the beam power shifts the position of this peak, demonstrating a possibility of tuning such lenses by varying either the beam power or the external field.

crystal orientation. In a negative-birefringence nematic, director tends to be perpendicular to the electric field, either static or optical. High intensity beams with transversal polarization thus effectively decrease the local angle of escape. In Fig. 3, we can see that high-intensity beams generally reduce the focusing, resulting in a larger spot size and a longer focus length. At very high laser powers, over 800 mW, the director becomes almost uniform (along the z direction – perpendicular to the polarization), resulting in a near-uniform refractive index.

If an external low-frequency electric field is applied in the z direction in a nematic with negative birefringence at this frequency, it rotates the director towards the xy plane, increasing the director angle and partially compensating for the reordering effects of the beam. Because

Optics EXPRESS

the external field is uniform, while the light intensity has a Laguerre-Gaussian profile, the compensation is spatially dependent. The competition between these forces can be summarized by the director and beam profiles in Fig. 3. The resulting birefringence profiles range from a fully open configuration with distortions only at the edges to a fully closed profile with a singular defect at the axis. In the case of high-intensity beams and a week external field (top right region of Fig. 3), the distortion is pushed away from the central axis of the escaped line and focusing is severely weakened. When the applied field is strong enough to overcome both the elastic forces and light intensity, the director is parallel to the polarization of light, and the light again observes a near-uniform refractive index (bottom left region of Fig. 3). However, the case where both effects are comparable, such as on the center image, exciting lensing director profiles emerge. The angle of escape plot shows strong spatial variations, as there is strong competition between the localized light beam and the uniform external field, in addition to elastic forces. Importantly, director variations are strong mainly in the area where light intensity is high, amplifying its effect on the beam.

Quality of lensing can be characterized by *numerical aperture*, computed as the half-angle of the cone of light exiting the lens. The effective beam diameter is computed as four times the standard deviation of the intensity distribution, in accordance with the ISO standard [50], and the cone angle is derived from the rate of change of the beam diameter. The plots in Fig. 4 show that numerical aperture drops steeply as the beam intensity is increased. In all cases, numerical aperture is not distinctly high comapred to standard lenses, because of the low birefringence and the different radial dependence of refractive index. However, the lenses described here are liquid, single-component, and tunable using either the beam itself or an external electric field.

By varying the external electric field and beam intensity, focusing can be adapted to very diverse regimes, allowing for effective tuning of such lenses. Figure 4 shows the director angle profile and the numerical aperture of the lens at different external field strengths and beam power. We see the effects of the competition between order elastic and the two external forces, as the director configurations range from mostly in the z directions to fully in the xy plane. Of special interest is the dependence of the numerical aperture on both beam power and external electric field, as shown in Fig. 4(c). At each beam power, there is a certain external field strength where focusing is strongest, and vice versa. This has important implications for tunability of such lenses: the numerical aperture can be tuned by changing the external field, or it can be self-tuned by changing the light beam intensity itself. Further, the lens can be constructed to focus only beams of a certain intensity range, and this range can be modified by changing the applied low-frequency electric field.

3.2. Waveguiding

Selective focusing properties of escaped director profiles can be used for polarization-dependent *waveguiding*. We find that narrow beams of radially polarized light travelling along an escaped line can follow the line, while beams with the opposite (azimuthal) polarization are not affected by the disclination. Thus escaped disclination lines can function as selective waveguides. A Laguerre-Gaussian beam with radial polarization introduced into an escaped-profile waveguide propagates along the guide with very low losses. Since the director profile has a radial symmetry, the waveguide mode is radially polarized as well. Notably, if a linearly polarized Gaussian beam is sent along an escaped profile, the beam diverges in the direction perpendicular to its polarization and no waveguiding is observed. This effect greatly depends on the scale of the escaped profile and material birefringence. The combination of $\Delta n = -0.05$ and $R = 1$ μm leads to the propagation as depicted in Fig. 5(a). When these two parameters are not tuned correctly, oscillations of the beam – known as “breathing” – are observed.

As seen in Fig. 5, the waveguide has a single distinct propagation mode. Different incident beams result in the same waveguide mode, while other components are quickly radiated out as

Optics EXPRESS

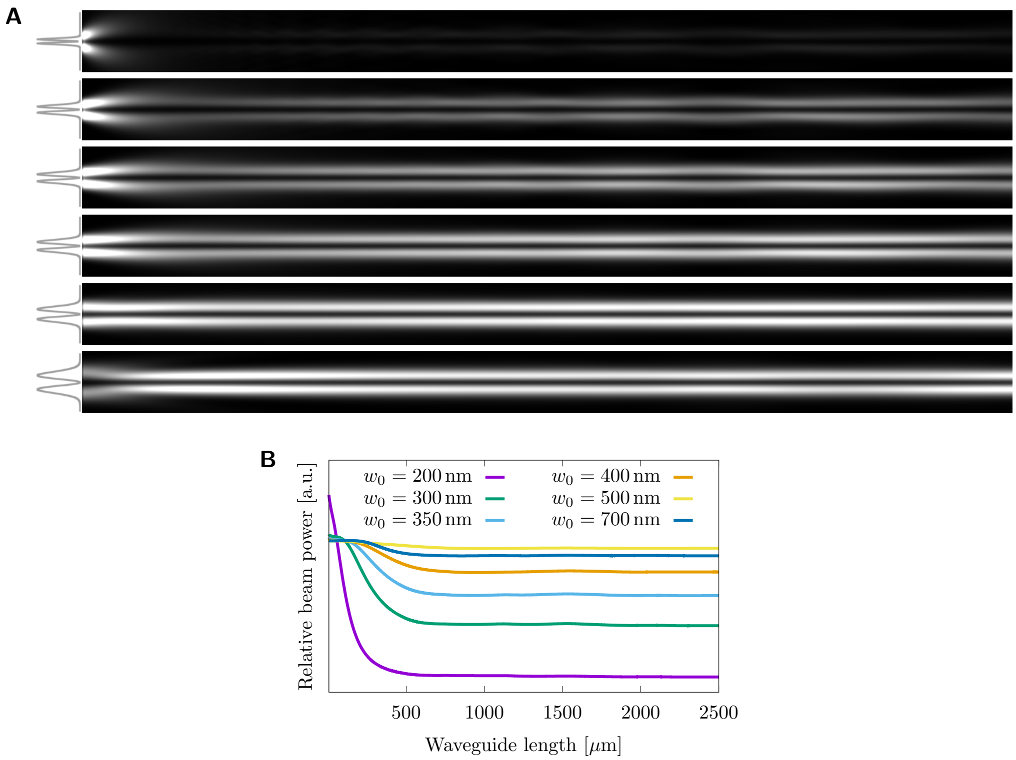

Fig. 5. Use of long escaped director profiles as waveguides. (A) Intensity profiles of incident beams of different widths show that the beams condense to the single eigenmode, which then remains stable for long distances. (B) Total beam power as a function of position inside the waveguide shows large initial losses, but confirms that the eigenmode is stable and the waveguide does not leak at larger distances. The magnitude of the losses depends on the incident beam width w_0.

losses. After this initial "shedding", the waveguide mode is stable with no noticeable losses on distances of up to 100 µm assuming no scattering or absorption in the material. As seen in Fig. 5(b), the beam intensity quickly drops when the beam enters the waveguide, but then stabilizes and remains nearly constant even over long distances. The initial intensity loss depends on how close the beam width is to the waveguide mode; in the case of the 500 nm beam, it is barely noticeable. For much wider and much narrower beams, however, most of their initial power is radiated as losses.

The intensity profile in the waveguide mode, shown in Fig. 5(c), appears rather similar to the Laguerre-Gaussian mode, and can be predicted analytically in the paraxial approximation. There are three independent variables defining the waveguide: capillary radius R, wavelength of light (represented by wave vector k) and the material optical dielectric anisotropy $\varepsilon_A = S\varepsilon_{\mathrm{a}}^{\mathrm{mol,opt}}$. Assuming radial polarization in the transversal plane and no modulation in the z direction, and substituting the ansatz $\mathbf{E} = E_0\psi(r)\mathbf{e}_r \exp(ikz - i\omega t)$ into the anisotropic Helmholtz equation, we obtain

$$\left[\nabla_\rho^2 + \frac{1}{\rho^2} + B\left(\frac{1-\rho^2}{1+\rho^2}\right)^2\right]\psi(\rho) = \beta\psi(\rho) \tag{1}$$

where $\rho = r/R$ is the reduced radius distance, $B = (kR)^2(n_e^2 - n_o^2)$ is a dimensionless waveguide

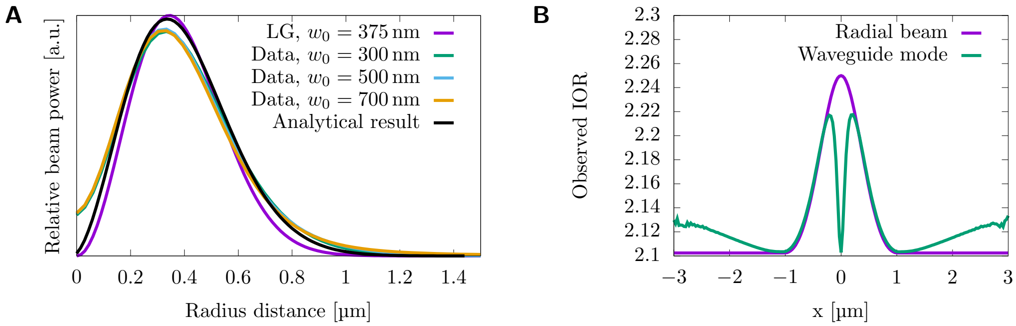

Fig. 6. (A) Cross-sections of the local light intensity show that the eigenmode is independent of the incident beam width w_0. A Laguerre-Gaussian profile is fitted to the mode, which gives a beam width of $w_0 = 375$ nm. Comparison to the Laguerre-Gaussian profile and the analytically obtained solution shows a discrepancy at the center, where simulation show nonzero intensity due to a presence of longitudinal polarization, while the analytic approaches assume zero intensity. (B) Spatial profile of the refractive index observed by the incident radially polarized beam and the stable waveguide mode. Discrepancies arise due to the presence of the longitudinal component at the center, as well as far away from the axis where the light intensity is very low.

parameter, and $\nabla^2_\rho = \frac{1}{\rho}\frac{\partial}{\partial\rho}(r\frac{\partial}{\partial\rho})$ is the radial part of the Laplacian. The equation can be discretized and solved numerically as an eigenvector problem for the field distribution $\psi(\rho)$, where the eigenvalue β is related to the mode's propagation velocity. The solution for parameters used in the numerical study is included in Fig. 6(a), which shows better matching with the numerical data than the incident Laguerre-Gaussian mode, especially in the longer tail, where the index of refraction in the escaped nematic profile deviates noticeably from the radius-squared relation. The most notable discrepancy is the nonzero intensity at the axis; this is prohibited by the assumption of transversal radial polarization. However, as seen from full numerical calculations (Fig. 6), the waveguide mode exhibits a longitudinal polarization component near the axis, as is common in focused radially polarized beams [51]. The longitudinal component causes the light to observe a different refractive index than it would otherwise, this difference is illustrated in Fig. 6(b). At the axis, the radial component is zero due to continuity of the electric field, so light is polarized fully in the z direction, parallel to the director near the axis, causing it to observe the lower extraordinary index of refraction. It thus appears that the presence of the longitudinal electric field is an important feature of radial birefringence profiles.

4. Conclusions

In conclusion, we show that the bulk nematic birefringent profile of a radial escaped line can perform as a polarization depended microlens and as a single-component fluid waveguide. The lensing is shown to vary with material birefringence; a negative birefringence material is needed to achieve converging lenses. The lens focusing can be well controlled by tuning the beam intensity or by an external electric field, combining self-lensing effects with external tunability. We further demonstrate that the same birefringence profiles can also guide light of a single distinct propagation mode with very low losses. Waveguiding is polarization dependent and is highly efficient on radially polarized light, whereas it has no effect on light of the opposite polarization. More generally, the presented nematic bulk birefringent profile lensing and waveguiding demonstrates the rich – and in many ways unexplored – interplay between elastic forces, confinement, external fields and light beams for use in photonics, where the unique combination of both internal and external control could lead to interesting phenomena, such as topology-driven light manipulation and controlling light with light. Combining such lenses and waveguides with polarization-modifying elements could allow for further control of light propagation, possibly leading to interesting applications in information processing and all-photonic circuits.

Funding

Slovenian Research Agency (Grant Z1-7300 and Programme P1-0099); U.S. Air Force AFRL EOARD Research Project "Nematic Colloidal Tilings as Tunable Soft Metamaterials."